Radiative Shocks in Rotating Accretion Flows around Black Holes

Toru Okuda

Hakodate College, Hokkaido University of Education, 1-2 Hachiman-cho, Hakodate 040-8567

okuda@cc.hokkyodai.ac.jp

and

V. Teresi, E. Toscano, and D. Molteni

Dipartimento di Fisica e Tecnologie, Universita di Palermo, Viale delle Scienza, Palermo, 90128, Italy

vteresi@unipa.it

(Received ; accepted)

Abstract

It is well known that the rotating inviscid accretion flows with adequate injection parameters around black holes could form shock waves close to the black holes, after the flow passes through the outer sonic point and can be virtually stopped by the centrifugal force. We examine numerically such shock waves in 1D and 2D accretion flows, taking account of cooling and heating of the gas and radiation transport. The numerical results show that the shock location shifts outward compared with that in the adiabatic solutions and that the more rarefied ambient density leads to the more outward shock location. In the 2D-flow, we find an intermediate frequency QPO behavior of the shock location as is observed in the black hole candidate GRS 1915+105.

Key words: accretion, accretion disks — black hole physics — shock waves — radiation — hydrodynamics

1. Introduction

Rotating inviscid and adiabatic accretion flow around a black hole under a pseudo-Newtonian potentials can have two saddle type sonic points. After the inviscid flow with adquate injection parameters passes through the outer sonic points, the supersonic flow can be virtually stopped by the centrifugal force, forming a standing shock close to the black hole and again falling into the black hole supersonically. @Apart from the initial works in the spherical transonic problems of accretion and wind, it was Fukue (1987) under a full relativistic treatment and Chakrabarti and his collaborators (Chakrabarti 1989 , Abramowicz, Chakrabarti 1990,

Chakrabarti, Molteni 1993) under a pseudo-Newtonian potential who were the first to provide the satisfactory analytical or numerical global shock solutions for transonic, invicid, rotating accretion around a Schwartzschild black hole. It has been shown that these generalized accretion flows could be responsible for the hard and soft state transitions or the quasi-periodic oscillation (QPO) of the hard X-rays from the black hole candidates (Molteni et al. 1996a, Ryu 1997, Lanzafame et al. 1998).

Recently, Das et al. (2001) examined analytically locations of sonic points and standing shocks in a thin, axisymmetric, adiabatic flow around a black hole and Das (2002) and Das (2003) showed that, using four available pseudo-Newtonian potentials, the standing shocks are essential ingredients in the multi-transonic black hole accretion disks. Using the generalized multi-transonic accretion model, Das et al. (2003a) and Das et al. (2003b) calculated analytically the QPO frequency of galactic black hole candidates in terms of dynamical flow variables and proposed a non-self-similar model of coupled accretion-outflow system in connection to QPO of the black hole powered galactic microquasars. Most of these analytical or numerical works of shocks in the rotating accretion flows around the black holes have been examined under the adiabatic condition, that is, the cooling and heating of gas and the radiation transport have not been taken account of. However, the radiation actually will play an important role in the overall flow structure, especially the shock location and the shocked temperatures. Accordingly it is worth-while to examine the shocks in the transonic black hole accretion disks, taking account of the radiation effects.

2. Model Equations

We examine these shock problems firstly in one-dimension and secondly in axisymmetric two-dimensional inviscid flow. A set of relevant equations consists of six partial differential equations for density, momentum, and thermal and radiation energy. These equations include the heating and cooling of gas and radiation transport. The radiation transport is treated in the gray, flux-limited diffusion approximation (Levermore, Pomraning 1981). Using cylindrical coordinates (r,z,φ), the basic equations for mass, momentum, gas energy, and radiation energy are written in the following conservative form:

$$\frac{\partial \rho}{\partial t} + \mathrm{div}(\rho \boldsymbol{v}) = 0, \tag{1}$$

$$\frac{\partial (\rho v)}{\partial t} + \mathrm{div}(\rho v \boldsymbol{v}) = \rho \left[\frac{v_\varphi^2}{r} - \frac{GM_*}{(\sqrt{r^2+z^2}-r_\mathrm{g})^2} \frac{r}{\sqrt{r^2+z^2}} \right] - \frac{\partial p}{\partial r} + f_r, \tag{2}$$

$$\frac{\partial (\rho w)}{\partial t} + \mathrm{div}(\rho w \boldsymbol{v}) = -\frac{\rho GM_*}{(\sqrt{r^2+z^2}-r_\mathrm{g})^2} \frac{z}{\sqrt{r^2+z^2}} - \frac{\partial p}{\partial z} + f_z, \tag{3}$$

$$\frac{\partial (\rho r v_\varphi)}{\partial t} + \mathrm{div}(\rho r v_\varphi \boldsymbol{v}) = 0, \tag{4}$$

$$\frac{\partial \rho \varepsilon}{\partial t} + \mathrm{div}(\rho \varepsilon \boldsymbol{v}) = -p\, \mathrm{div} \boldsymbol{v} - \Lambda, \tag{5}$$

and

$$\frac{\partial E_0}{\partial t} + \mathrm{div}\boldsymbol{F_0} + \mathrm{div}(\boldsymbol{v}E_0 + \boldsymbol{v}\cdot P_0) = \Lambda - \rho\frac{(\kappa+\sigma)}{c}\boldsymbol{v}\cdot\boldsymbol{F_0}, \tag{6}$$

where ρ is the density, $\boldsymbol{v} = (v, w, v_\varphi)$ are the three velocity components, G is the gravitational constant, M_* is the central mass, p is the gas pressure, ε is the specific internal energy of the gas, E_0 is the radiation energy density per unit volume, and P_0 is the radiative stress tensor. It should be noticed that the subscript "0" denotes the value in the comoving frame and that the equations are correct to the first order of $\boldsymbol{v}/c$ (Kato et al. 1998). We adopt a pseudo-Newtonian potential (Paczyński, Wiita 1980) in equations (2) and (3), where $r_{\rm g}$ is the Schwartzschild radius given by $2GM_*/c^2$. The force density $\boldsymbol{f}_{\rm R} = (f_r, f_z)$ exerted by the radiation field is given by

$$\boldsymbol{f}_{\rm R} = \rho\frac{\kappa+\sigma}{c}\boldsymbol{F_0}, \tag{7}$$

where κ and σ denote the absorption and scattering coefficients and $\boldsymbol{F_0}$ is the radiative flux in the comoving frame. For one-dimensional form, we put z=0 in equation (2) and omit equation (3).

The quantity Λ describes the cooling and heating of the gas, i.e., the energy exchange between the radiation field and the gas due to absorption and emission processes,

$$\Lambda = \rho c\kappa(S_* - E_0), \tag{8}$$

where S_* is the source function and c is the speed of light. For this source function, we assume local thermal equilibrium $S_* = aT^4$, where T is the gas temperature and a is the radiation constant. For the equation of state, the gas pressure is given by the ideal gas law, $p = R_{\rm G}\rho T/\mu$, where μ is the mean molecular weight and $R_{\rm G}$ is the gas constant. The temperature T is proportional to the specific internal energy, ε, by the relation $p = (\gamma-1)\rho\varepsilon = R_{\rm G}\rho T/\mu$, where γ is the specific heat ratio. To close the system of equations, we use the flux-limited diffusion approximation (Levermore, Pomraning 1981) for the radiative flux:

$$\boldsymbol{F_0} = -\frac{\lambda c}{\rho(\kappa+\sigma)}\mathrm{grad}\ E_0, \tag{9}$$

and

$$P_0 = E_0 \cdot T_{\rm Edd}, \tag{10}$$

where λ and $T_{\rm Edd}$ are the *flux-limiter* and the *Eddington Tensor*, respectively, for which we use the approximate formulas given in Kley (1989). The formulas fulfill the correct limiting conditions in the optically thick diffusion limit and the optically thin streaming limit, respectively.

3. Model Parameters and Numerical Methods

For the central black hole, we assume a Schwartzschild black hole with mass $M_* = 10M_\odot$. We try to find the steady solutions with shocks by solving the time-dependent equations (1)–(6),

Table 1. Injection Parameters

Case	$v_{\rm out}$	$a_{\rm out}$	$\lambda_{\rm out}$	$\epsilon_{\rm out}$	$R_{\rm in}/R_{\rm g}$	$R_{\rm out}/r_{\rm g}$	ϕ
1D	0.0751	0.0564	1.875	0.0075	2.0	100	–
2D	0.0938	0.0738	1.64	0.005	1.5	30	29°

which are numerically integrated by a finite-difference method under initial and boundary conditions. To do this, we have to determine the injection parameters such as the specific angular momentum $\lambda_{\rm out}$, the radial velocity $v_{\rm out}$, and the sound velocity $a_{\rm out}$ at an outer boundary radius $R_{\rm out}$, whose parameters can lead to a shock wave close to the black hole. We search analytically these injection parameters through the examination of the paremeter space (ϵ, λ), where ϵ and λ are the total specific energy and the specific angular momentum (e.g. Chakrabarti 1989,Molteni et al. 1994, Molteni et al. 1999). Typical injection parameters for 1D and 2D flows obtained thus are listed in table 1. Here, the velocities and distances are given in units of the speed of light c and the Schwartzschild radius $r_{\rm g}$, respectively. ϕ is the subtended angle of the centeral star to the initial disk at $r = R_{\rm out}$, that is, $\tan\phi = (h/r)_{\rm out}$, where h is the disk thickness. 2D case in the table corresponds to a super-Eddington accretion with an accretion rate $\dot{M} \sim 10^{20}$ g s^{-1} which is $\sim 64\dot{M}_{\rm E}$ for the Eddington luminosity $L_{\rm E} = \dot{M}_{\rm E}c^2$, where $\dot{M}_{\rm E}$ is the Eddington critical accretion rate, and the ambient density $\rho_{\rm out}$ is taken to be 1.25×10^{-6} g cm^{-3}.

At the outer boundary radius the injection parameters are always kept constantly. At the inner boundary radius $R_{\rm in}$, a supersonic radial velocity is specified. Adequate initial conditions of isothermal temperature and adequate r-dependent distribution of density are imposed on the flow. With these initial and boundary conditions, we perform time integration of equations (1)–(6) until the steady solutions are obtained. The numerical schemes used are basically the same as that described previously (Kley 1989,Okuda et al. 1997) but with no viscosity description.

4. Numerical Results

4.1. One-Dimensional Flows

Firstly, under the injection parameters in Table 1, we numerically obtained a steady adiabatic shock with an ambient density $\rho_{\rm out} = 3.5 \times 10^{-5}$ g cm^{-3} at the outer boundary $r = R_{\rm out}$. If a set of the injection parameters are given, the shock position in the adiabatic case is independent on the ambient density, because the basic equations of the adiabatic and inviscid flow are almost independent on the density as far as the ideal gas law is used. However, in the non-adiabatic cases, we obtain steady or sometimes nonsteady shock structure dependent on the ambient density and the shock locations are also dependent on the ambient density. Figure 1 show the numerical results of density (a), temperature (b), radial velocity (c), and Mach number (d) of the velocity in the adiabatic flow (A) and non-adiabatic flows with different ambient densities of $\rho_{\rm out} = 3.5 \times 10^{-5}$ (B), 3.5×10^{-6} (C), 7.0×10^{-7} (D) g cm^{-3}, respectively.

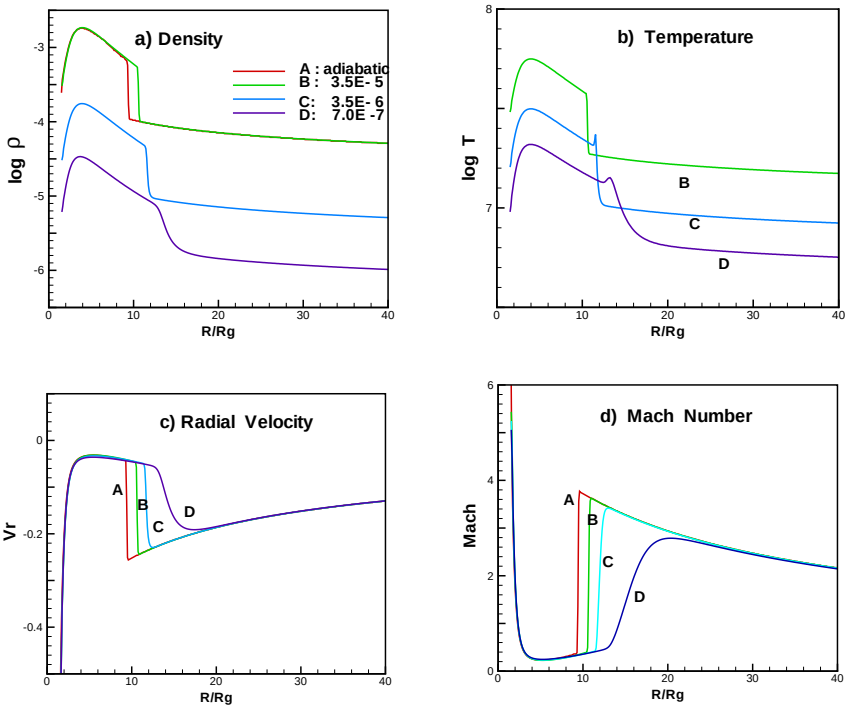

Fig. 1. Flow structures in one dimensions with shock waves: (a) density ρ: red line (A) shows the structure in adiabatic case with $\rho_{\rm out} = 3.5 \times 10^{-5}$ g cm^{-3}, and green (B), blue (C), and dark blue (D) lines denote the structures of non-adiabtic case with $\rho_{\rm out} = 3.5 \times 10^{-5}, 3.5 \times 10^{-6}$, and 7.0×10^{-7}, (b) temperature T: case A is not included here, because the temperatures in case A are very hot as $\sim 10^{10}$ – 10^{11} K, (c) radial velocity v, (d) Mach number of the velocity v.

The numerical results in the adiabatic flow agree well with the analytical ones, where the shock locates at $r = 9.4 r_{\rm g}$.

The shocked temperatures in the adiabatic flow are too high to be $\sim 10^{10}$ – 10^{11} K, while actual postshock temperatures in B, C, and D are rather low as 2 – 5 $\times 10^7$ K. The large temperature differences are attributed to the differences of the temperatures specified initially at the outer boundary, where same injection parameters of the sound velocity $a_{\rm out}$ and the radial velocity $v_{\rm out}$ are used in the adiabatic and non-adiabatic cases. If an optically thick and radiation-pressure dominant accretion flow is considered in the non-adiabatic case, we have

$$(a_{\rm out} * c)^2 = [R_{\rm G} T_{\rm ad}/\mu]_{\rm adiabatic} = \left[a T_{\rm nad}^4/3\rho_{\rm out}\right]_{\rm non-adiabatic}, \tag{11}$$

where $T_{\rm ad}$ and $T_{\rm nad}$ are the temperatures at the outer boundary in the adiabatic and non-adiabatic cases, respectively. Therefore, for a given $a_{\rm out}$, we have smaller $T_{\rm nad}$ for smaller ambient density $\rho_{\rm out}$ and, under the injection parameter $a_{\rm out} = 0.0564$ in 1D-flow with $\rho_{\rm out} = 3.5 \times 10^{-5}$ g cm^{-3}, $T_{\rm ad} \sim 2 \times 10^{10}$ K and $T_{\rm nad} \sim 1.4 \times 10^7$ K. $T_{\rm ad}$ is three orders of magnitude larger than $T_{\rm nad}$. Although the temperature profile in the non-adiabatic case is dependent on the ambient density, the radial velocities and their Mach numbers take the radial profiles

independent on the ambient density in the pre-shock region, as is found in Figure 1-(c) and (d).

Figure 1 also shows that the more rarefied ambient density the flow has, the shock position moves more outward and the shock thickness becomes broader. The shock locations shift to 10.6, 12.0, and ~ 15, in cases B, C, and D, respectively. If the ambient density $\rho_{\rm out}$ is too low as $\sim 3.5 \times 10^{-7}$ g cm^{-3}, the steady shock does not exist finally. At the Rankine-Hugoniot relation of a standing shock, the pressure balance is supported by the dominant radiation pressure and the ram pressure in the present non-adiabatic case. If the ambient density is taken to be smaller than that at a standing shock, the pressure at the upstream just before the shock becomes much smaller because of the lower temperature in the pre-shock region. Therefore, to set up a new pressure balance condition at the shock, the shock must shift outward as far as the same injection parameters are concerened. When the shock position shifts more outward, the Mach number of the pre-shock velocity decreases, that is, the shock becomes weaker. Generally the shock thickness is inversely proportional to the wave strength, and the scale factor is the radiation mean free path in our case. Therefore the shock broadens gradually with decreasing ambient densities. If the ambient density is too low, it may be imposibble to establish the Rankine-Hugoniot shock conditions in the region considered and the shock disappears.

4.2. Two-Dimensional Flows

Figures 2 and 3 show the temperature contours for 2D adiabatic and nonadiabatic accretion flows, respectively, under the injection parameters in Table 1 and the ambient density $\rho_{\rm out} = 1.25 \times 10^{-6}$ g cm^{-3} at the outer boundary.

There are generally two important features of a two-dimensional rotating accretion flow around a black hole. One is the funnel wall, which is roughly characterized by a surface $(x_{\rm f}, z_{\rm f})$ of vanishing effective potential

$$\Phi_{\rm eff} = \frac{-1}{(r_{\rm f} - 1)} + \frac{\lambda^2}{{x_{\rm f}}^2} = 0, \tag{12}$$

where $r_{\rm f} = (x_{\rm f}^2 + z_{\rm f}^2)^{1/2}$. The other is the centrifugal barrier $(x_{\rm cf}, z_{\rm cf})$, which is governed by the competition between the centrifugal force and gravitational force

$$\frac{-1}{(r_{\rm cf} - 1)^2} + \frac{\lambda^2}{x_{\rm cf}^3} = 0. \tag{13}$$

In the adiabatic flow, the standing shock appears at $r/r_{\rm g} = 9.3$ on the equatorial plane and is bent upward toward the upstream, roughly following the contour of the centrifugal barrier. The post-shock temperatures are as high as $\sim 10^{10}$ – 10^{11} K as is found in 1D case. In the red and yellow regions between the rotating axis and the funnel wall, the temperatures are much higher and the densities are very low and in these regions the outflow gas with high velocities are formed. These results are similar to that by the previous TVD and SPH simulations (Molteni

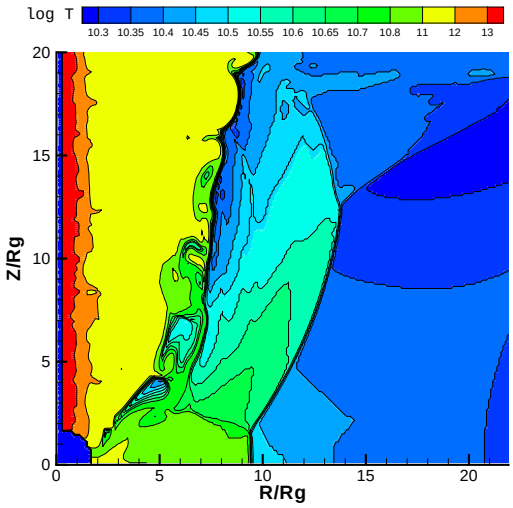

Fig. 2. Temperature contours in two-dimensional adiabatic flow with shock wave. The steady shock is formed at $r/r_{\rm g} \sim 9.3$ near the equatorial plane and the shock front indicated by the thick black lines extends obliquely to the upstream.

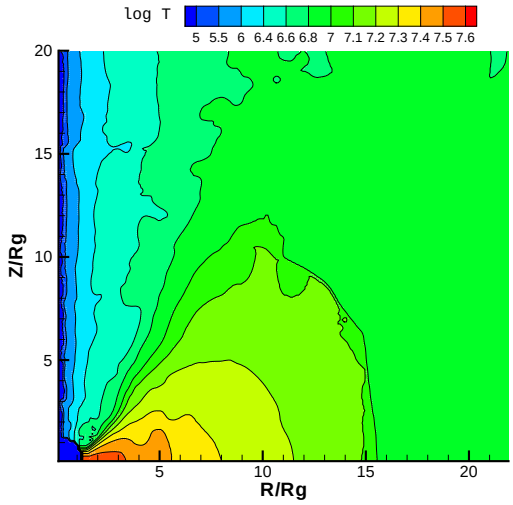

Fig. 3. Same as figure 2 but here the cooling and heating of the gas and the radiation transport are taken account of. In this figure, the shock appears at $r/r_{\rm g} \sim 15$ near the equatorial plane but is not steady, and its position oscillates between $12 \leq r/r_{\rm g} \leq 17$.

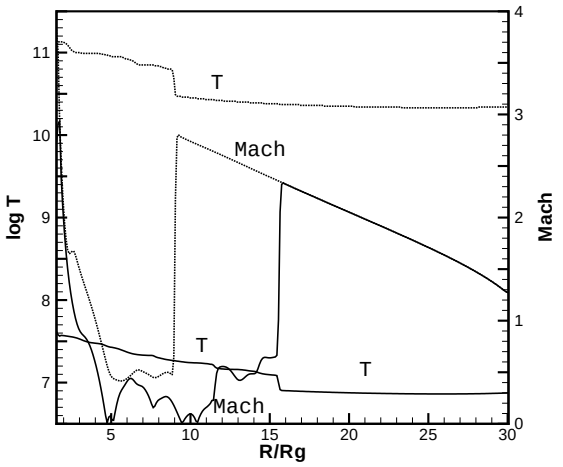

Fig. 4. Profiles of the temperature and the Mach number of the radial velocity on the equatorial plane for 2D adiabatic (dotted lines) and nonadiabatic (solid lines) flows.

et al. 1996b) in the 2D adiabatic flow.

In contrast to the adiabatic flow, when the cooling and heating of gas and the radiation are taken account of, a spheroidal shock is formed between the funnel wall and the equatorial plane and the shock oscillates quasi-periodically. Figure 3 shows the temperature contours at the evolutionary time $t = 5.5 \times 10^4 r_{\rm g}/c$ in the non-adiabatic flow where the shock appears at $r_{\rm s} \sim 15 r_{\rm g}$ on the equatorial plane. The overall flow is optically thick except the cone-like funnel region between the funnel wall and the rotational axis. In the funnel region we have very rarefied and optically thin flow but the temperatures are not so high compared with the high temperatures in the viscous accretion flows where the viscously dissipative energy heats up considerably (Okuda 2002). As a result, a relativistically high velocity jet is not formed here in spite of the high input accretion rate. The temperatures in the shocked region are 1 – 4 $\times 10^7$ which are three orders of magnitude smaller than that in the adiabtic flow. For clearness of the shock location and the shocked temperature, in figure 4 we plot the temeprature and the mach number of the radial velocity on the equatorial plane. It is clear that the effects of radiation shifts the shock position $r_{\rm s} \sim 9 r_{\rm g}$ to $\sim 15 r_{\rm g}$ and the shock strength weakens.

The shock in figure 3 oscillates and this induces the luminosity fluctuations. Figure 5 shows the shock radii on the equatorial plane and the luminosity as a function of time in units of $r_{\rm g}/c$. Although the time variation of the shock position on the equatorial plane is complicated, we find that it oscillates quasi-periodically with a period of $\sim 2000 r_{\rm g}/c$ (0.2 sec) and its frequency $\nu \sim$ 5Hz. The spheroidal shock also oscillates in the similar way but the luminosity shows a more complicated variation due to the convective nature and the geometry of 2D-flow.

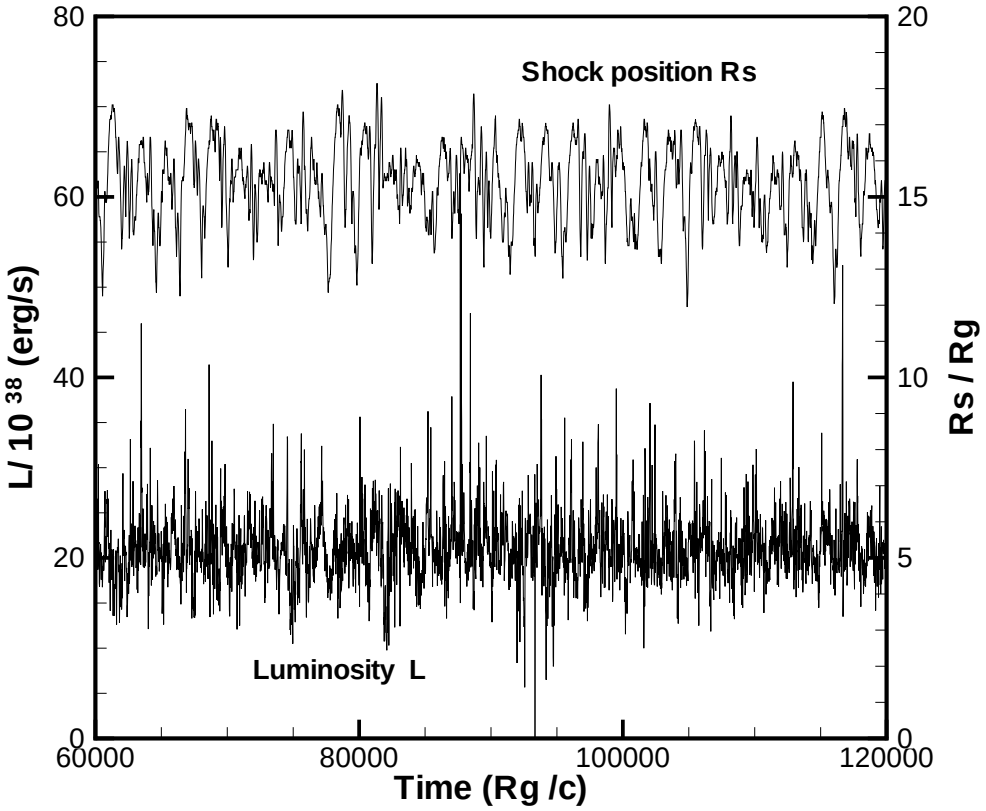

Fig. 5. Shock location and luminosity versus as a function of time in units of $r_{\rm g}/c$ in 2D nonadiabatic flow.

5. Discussion and Conclusion

In the present paper, we have numerically examined 1D and 2D inviscid transonic flows, taking account of the cooling and heating of gas and radiation transport. As the results, we find that the location of the centrifugally driven shock drifts more outward from the black hole compared with that in the adiabatic flow and that the postshock temepratures are as high as $1 - 4 \times 10^7$ K which is three orders of magnitude lower than that in the adiabatic flow. When a set of the injection parameters such as the specific angular momentum λ, the radial velocity $v_{\rm out}$, and the sound velocity $a_{\rm out}$ at the outer boundary are specified, the more rarefied ambient density the flow has, the shock location drifts more outward. When the ambient density is too low, the shock wave exists no longer under the injection parameters. Depending on the injecteion parameters, even if the shock wave exists, it becomes sometimes unstable, that is, the shock location oscillates.

The transonic accretion shocks around the black holes have been applied to

the hard and soft spectral states observed in the black hole candidates (Chakrabarti, Titarchuk 1995,Chakrabarti 1997). In the shock model, the accretion disk is decomposed into three distinct components : (1) an optically thick Keplerian disk on the equatorial plane ($r > r_{\rm s}$); (2) a sub-Keplerian optically thin halo above the disk ($r > r_{\rm s}$); (3) a hot, optically slim post-shock region ($r < r_{\rm s} \sim 5$ – $10 r_{\rm g}$). The hot, dense post-shock region intercepts soft photons from a pre-shock region and a cold outer accretion disk and reprocesses them to form high-energy photons. This model seems to explain well the observed properties. In this respect, our results of the radiative shock may have such observational appearance in black-hole candidates. Molteni et al. (1996a) and Lanzafame et al. (1998) have examined shock waves in the viscous accretion disks around black holes and showed that when the viscosity parameter α is less than a critical value, standing shock waves are formed but that if the viscosity is high then the shock wave dissapears. Also in our 1D-cases, we confirmed that the standing shock is formed for small α and that the shock position drifts more outward for larger viscosity parameter until it attains to $\sim 10^{-4}$.

The shocked accretion flows have been applied to the QPO phenomena in galactic black hole candidates. The galactic X-ray transient source GRS 1915+105 exhibits various types of quasi-periodic oscillations with frequencies ranging from ~ 0.001 – 10 Hz to ~ 67 Hz (Morgan 1997). Analyzing X-ray data in GRS 1915+105, Rao (2000) showed that a thermal-Compton spectrum is responsible for the QPO generation and supported the hypothesis that the QPO is generated by the oscillation of the shock front in the transonic accretion flow. The QPOs are classified as (1) the low-frequency QPO ($\nu_{\rm L} \sim 0.001$ – 0.01Hz), (2) the intermediate frequency QPO ($\nu_{\rm I} \sim 1$ – 10Hz), and (3) the high frequency QPO ($\nu_{\rm H} \sim 67$ Hz). The QPO-like behavior of the shock oscillations with $\nu \sim 5$ Hz in our 2D-flow may be representative of the intermediate frequency QPO observed in GRS 1915+105. The oscillation amplitude of the shock location could be up to 15 % of the distance of the shock wave from the black hole. This results in a quasi-periodic behavior of the luminosity with an amplitude variation of a factor 2. However we are not able to find distinctly these frequency peaks of $\nu_{\rm I}$, $\nu_{\rm L}$, and $\nu_{\rm H}$ from the power spectra of the luminosity curve.

Molteni et al. (1996a) have found the QPO behaviors in viscous accretion disks with shock waves around a black hole with $M = 10^8 M_\odot$. They obtained stable shock oscillations with periods of 1500 – 2000 in units of $r_{\rm g}/c$, which depends on an index of power-law cooling function of gas. The oscillation period $t_{\rm osc}$ of 1500 units in the case of bremsstrahlung cooling is comparable to 2000 units in our case. On the other hand, they interpreted the oscillation period as the advection timescale $t_{\rm adv}$ only when it is comparable to the cooling timescale of the flow and estimate it as follows:

$$t_{\rm osc} \sim t_{\rm adv} = \int_1^{r_{\rm s}} \frac{dr}{v_+}, \tag{14}$$

where v_+ is the post-shock velocity. If the pre-shock velocity v_- at the shock is taken to be

a fraction f of the free-fall velocity, $t_{\rm osc} = Rr_{\rm s}^{3/2}/f$ where R is the compression ratio of gas at the shock. Using $r_{\rm s}/r_{\rm g} = 17$, R= 7, and f =0.7 estimated in our results, we have $t_{\rm osc} \sim$ 700 units which is smaller by a few factor than actual 2000 units. If a post-shock flow of constant velocity $v_+ = v_0/R$ is used, where v_0 is a fraction of the speed of light, $t_{\rm osc} = R\, r_{\rm s}/v_0$. For $r_{\rm s} = 17, R = 7$, and $v_0 = 0.066$, we have $t_{\rm osc}$ = 1800 units (0.17 sec) and a frequency of $\nu \sim 6$ Hz which corresponds to the shock oscillation frequency in our 2D-flow. Assuming an outflow from the post-shock region , Chakrabarti (1999) derived a correlation between the shock location and the duration of the quiescence state of GRS 1915+105 with typical QPOs and Chakrabarti,Manickam (2000) showed that the correlation with $v_0 = 0.066$ was well fitted to public-domain data from RXTE. These transonic shock wave models in rotating accretion flows around black holes may be promissing for the explanation of the QPOs in the black hole candidates.Further examinations of the models are required from a 2D-simulation point of view.

References

Abramowicz, M., & Chakrabarti, S. K., 1990, ApJ, 350, 281

Chakrabarti, S. K., 1989, ApJ, 347, 365

Chakrabarti, S. K., 1997, ApJ, 484, 313

Chakrabarti, S. K., 1999, A&A, 351, 185

Chakrabarti, S. K., & Manickam, S. G., 2000, ApJL, 531, L41

Chakrabarti, S. K., & Molteni, D., 1993, ApJ, 417, 671

Chakrabarti, S. K., & Titarchuk, L. G., 1995, ApJ, 455, 623

Das, S., Chattopadhyay, I., & Chakrabarti, S., 2001, ApJ, 557, 983

Das, T. K., 2002, ApJ, 577, 880

Das, T. K., 2003, ApJ, (astro-ph/0302014)

Das, T. K., Pendharkar, J. K., & Mitra, S., 2003a, ApJ, (astro-ph/0301189)

Das, T. K., Rao, A. R., & Vadawale S. V., 2003b, MNRAS, (astr-ph/0301344)

Fukue, J., 1987, PASJ, 39, 309

Kato, S., Fukue, J., & Mineshige, S. 1998, Black Hole Accretion Disks (Kyoto: Kyoto University Press)

Kley, W. 1989, A&A, 208, 98

Lanzafame, G., Molteni, D., & Chakrabarti, S. K. 1998, MNRAS, 299, 799

Levermore, C. D., & Pomraning, G. C. 1981, ApJ, 248, 321

Molteni, D., Lanzafame, G., & Chakrabarti, S. K. 1994, ApJ, 425, 161

Molteni, D., Sponholz, H., & Chakrabati, S. K. 1996a, ApJ, 457, 805

Molteni, D., Ryu, D., & Chakrabarti, S. K. 1996b, ApJ, 470, 460

Molteni, D., Toth, G., & Kuznetsov, O. 1999, ApJ, 516, 411

Morgan, E. H., Remillard, R. A., & Greiner, J., 1997, ApJ, 482, 993

Okuda, T., Fujita, M., & Sakashita, S. 1997, PASJ, 49, 679

Okuda, T., 2002, PASJ, 54, 253

Paczyńsky, B., & Wiita, P. J. 1980, A&A, 88, 23
Rao, A. R., Naik, S., Vadawale, S. V., & Chakrabarti, S. K., 2000, A&A, 360, L25
Ryu, D., Chakrabarti, S. K., & Molteni, D., 1997, ApJ, 474, 378